Journal of Materials Chemistry C

Accepted Manuscript

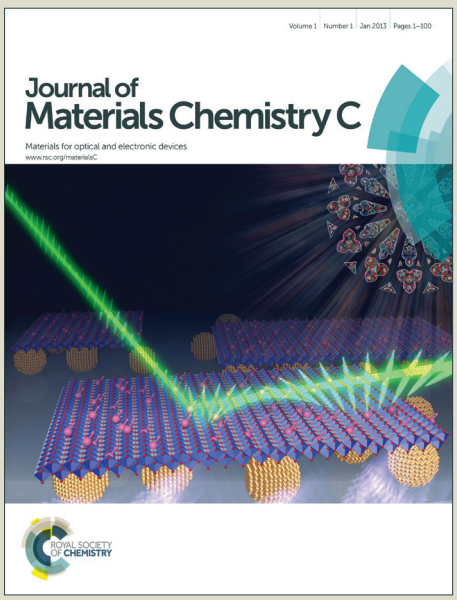

ROYAL SOCIETY OF CHEMISTRY

www.rsc.org/materialsC

Cite this: DOI: 10.1039/c0xx00000x

www.rsc.org/xxxxxx

ARTICLE TYPE

$KMnF_3$: Yb^{3+}, Er^{3+} @ $KMnF_3$: Yb^{3+} active-core-active-shell nanoparticles with enhanced red up-conversion fluorescence for polymer-based waveguide amplifiers operating at 650nm

Yongling Zhang,[1] Fei Wang,[1] Yanbo Lang, Jiao Yin, Meiling Zhang, Xiaohui Liu, Daming Zhang, Dan Zhao*, Guanshi Qin*, Weiping Qin*

[1]These authors contributed equally to this work.

Received (in XXX, XXX) Xth XXXXXXXXX 20XX, Accepted Xth XXXXXXXXX 20XX
DOI: 10.1039/b000000x

We demonstrated optical amplification at 650 nm in $KMnF_3$: Yb^{3+}, Er^{3+} @ $KMnF_3$: Yb^{3+} active-core-active-shell nanoparticles (NPs) doped polymer waveguides pumped by a 976 nm laser diode for the first time. $KMnF_3$: Yb^{3+}, Er^{3+} NPs were synthesized via a solvothermal method. With the excitation of a 976 nm laser diode, bright red upconversion (UC) fluorescence was observed from $KMnF_3$: Yb^{3+}, Er^{3+} NPs owing to the existence of efficient energy transfer between Er^{3+} and Mn^{2+}: $^2H_{11/2}$, $^4S_{3/2}+^6A_1 \rightarrow ^4I_{15/2}+^4T_1$, $^2H_{9/2}+^6A_1 \rightarrow ^4I_{13/2}+^4T_1$ and $^4I_{15/2}+^4T_1 \rightarrow ^4F_{9/2}+^6A_1$. The red UC emissions originated from the $^4F_{9/2} \rightarrow ^4I_{15/2}$ transition of Er^{3+}. Furthermore, the red UC emissions of $KMnF_3$: 18 mol% Yb^{3+}, 1 mol% Er^{3+} @ $KMnF_3$: 2 mol% Yb^{3+} NPs were enhanced by 7.5 times compared to that of $KMnF_3$: 18 mol% Yb^{3+}, 1 mol% Er^{3+} core-only NPs after coating an active shell containing Yb^{3+} ions on the core-only NPs. The above results showed that the active-shell could be used to not only suppress surface quenching but also transfer the pump light to the core region efficiently through Yb^{3+} ions inside the active-shell. By using $KMnF_3$: 18 mol% Yb^{3+}, 1 mol% Er^{3+} @ $KMnF_3$: 2 mol% Yb^{3+} NPs as the gain medium and doping NPs into a polymer waveguide, we constructed polymer-based waveguide amplifiers. For an input signal power of 7.4 mW and a pump power of 45.2 mW, a relative optical gain of ~ 3.5 dB was obtained at 650 nm in a 17 mm-long waveguide.

1 Introduction

Since lanthanide-doped upconversion (UC) nanoparticles (NPs) can be used to convert long wavelength light to short wavelength light via the sequential absorption of two or more photons through intermediate energy levels, UCNPs are applied in a number of fields, such as solar battery,[1] photo-catalysis,[2] three-dimensional displays,[3] and biomedicine[4-6] (e.g., bioimaging biolabeling, and photodynamic therapy). Recently, many efforts have been devoted to improving the performance of UCNPs because of their low luminescence efficiency caused by the surface quenching effect. One practical strategy is using core-shell architectures, where inert shells or active shells with similar lattice constants are grown around the core NPs and can prevent the surface defect from interaction with lanthanide ions.[7-16] Despite recent progress in this field, one of the optical properties of UCNPs previously a little considered but now recognized as potentially useful is the optical gain. Optical gain is a measure of the ability of an optical amplifier to increase the power or amplitude of an optical signal from the input to the output by adding energy converted from some power supply to the signal. By dispersing UCNPs in an optical fiber or waveguide, optical fiber or waveguide amplifiers can be constructed and used in various fields, such as telecommunications, sensing, and optical instrumentation.[17,18] Since UCNPs with strong UC fluorescence can be synthesized by flexible design of composition, phase structure,[19-21] it is very important to explore the potential of UCNPs for constructing optical amplifiers operating at short wavelengths. The potential application of visible optical amplifiers is to overcome the loss in automobile optical local area networks (LANs).[22] In recent years, to meet the requirements of high-speed information transmission in the aspects of automobile technology, automobile optical LANs have been developed rapidly. The combination of plastic optical fibers and visible light-emitting diode played an important role in the field of automobile optical LANs owing to its low-loss in the visible light region and low cost of plastic optical fibers.[23] Optical amplification is still necessary when the optical signal is distributed, although automobile optical LAN is a short-distance optical communication system.

In recent years, since polymethyl methacrylate (PMMA) polymers have a low loss in visible wavelength region and are relatively cheap, there is an increased interest in constructing PMMA polymer optical amplifiers.[24] For example, a signal gain of ~5.7 dB at 613 nm was obtained for a 30 cm long device using

[Eu(DBM)$_3$(Phen)]-doped PMMA polymer fiber.[25] However, in those works, ultra-violet light was commonly used as pumping source,[25-27] if the waveguide amplifiers were exposed under ultra-violet light for a long time, the organic matrix would be damaged. It was an efficient way to resolve the above problem by using UCNPs doped polymer waveguide amplifiers. The UCNPs can absorb near infrared (NIR) light and emit visible light. The NIR light causes little damage to the devices. To our best knowledge, visible optical waveguide amplifiers based on UCNPs have not yet been reported.

In this paper, we reported optical amplification at 650 nm in a polymer waveguide amplifier based on $KMnF_3$: Yb^{3+}, Er^{3+} @ $KMnF_3$: Yb^{3+} active-core-active-shell NPs for the first time. A relative optical gain of ~ 3.5 dB was obtained at 650 nm in a 17 mm-long waveguide pumped by a 976 nm laser diode (LD) with a power of 45.2 mW.

2 Materials and Methods

2.1 Materials and general procedures

99.99% $YbCl_3$•$6H_2O$ and 99.9% $ErCl_3$•$6H_2O$ were obtained from Beijing Chemicals Reagents. Oleic acid (OA) was purchased from Alfa Aesar Company. $MnCl_2$•$4H_2O$ (98%), KOH (98%), KF (99%), Methylmethacrylate (MMA), and ethanol were bought from Beijing Fine Chemical Company. All other reagent were used without further operation.

2.2 Synthesis of $KMnF_3$: 18 mol% Yb^{3+}, 1 mol% Er^{3+} Core Nanocrystals

5 ml of deionized water and 12 mmol KOH were added into a 50 mL beaker containing 10 ml OA and 5 ml ethanol under stirring at room temperature (RT). $MnCl_2$ (0.324 mmol), $YbCl_3$ (0.072 mmol) and $ErCl_3$ (0.004 mmol) and KF (3.5 mmol) were added into 50 mL beaker under stirring for 0.5 hour. Finally, the solution was heated to 200 °C and kept for 1 h. The production was cooled to RT naturally. These NPs were acted as cores for subsequent shell coating (shown in **Fig. S1**).[28,29]

2.3 Synthesis of $KMnF_3$: 18 mol% Yb^{3+}, 1 mol% Er^{3+} @ $KMnF_3$: 2 mol% Yb^{3+} Core−Shell Nanoparticle

5 ml of deionized water and KOH (12 mmol) were added to a 50 mL beaker containing 10 ml OA and 5 ml ethanol under stirring at RT. $MnCl_2$ (0.392 mmol) and $YbCl_3$ (0.008 mmol) were added into 50 mL beaker under stirring for 0.5 hour. Then the core-only NPs was added to the system under stirring for 0.5 hour. Later, KF (3.5 mmol) was added to the system under stirring for 0.5 hour. Finally, the solution was heated to 200 °C and kept for 12 h. The solution was cooled to RT naturally. The core-shell NPs was washed with ethanol and cyclohexane via centrifugalization (shown in **Fig. S2**).[30,31]

2.4 Characterization

The crystalline phase of these samples was performed by X-ray powder diffraction (XRD) (Model Rigaku Ru-200b), using a nickel-filtered Cu-K α radiation in the scope of $10° \leq 2\theta \leq 70°$ (λ = 1.5406 Å). The morphology of these samples was analyzed by a JEM-2100F electron microscope and scanning electron microscope. FT-IR (Fourier Transform infrared spectroscopy) spectra were measured with a BioRad Fourier transform infrared spectrometer, using the KBr method. The fluorescence spectrum were obtained by a Hitachi F-4500 fluorescence spectrophotometer, using a 976 nm laser device as the excitation source at Room Temperature (RT). The lifetime of these samples was measured by using a 953.6 nm Raman shifter laser and an oscillograph at RT.

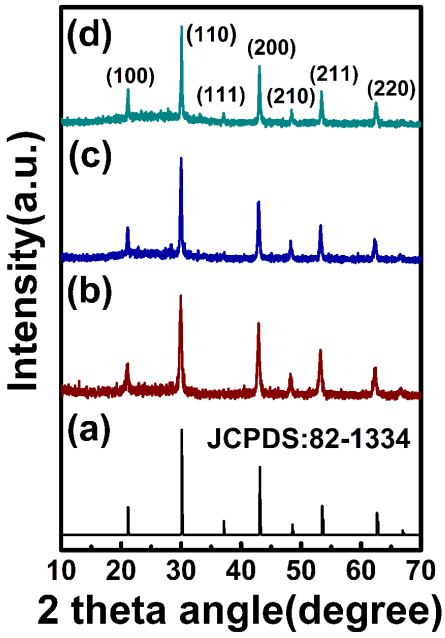

Fig. 1 XRD patterns of (a) standard KMnF3 NPs, (b) $KMnF_3$: 18 mol% Yb^{3+}, 1 mol% Er^{3+} core-only NPs, (c) $KMnF_3$: 18 mol% Yb^{3+}, 1 mol% Er^{3+} @ $KMnF_3$ active-core- inert -shell NPs, (d) $KMnF_3$: 18 mol% Yb^{3+}, 1 mol% Er^{3+} @ $KMnF_3$: 2 mol%Yb^{3+} active-core-active-shell NPs.

Cite this: DOI: 10.1039/coxx00000x

www.rsc.org/xxxxxx

ARTICLE TYPE

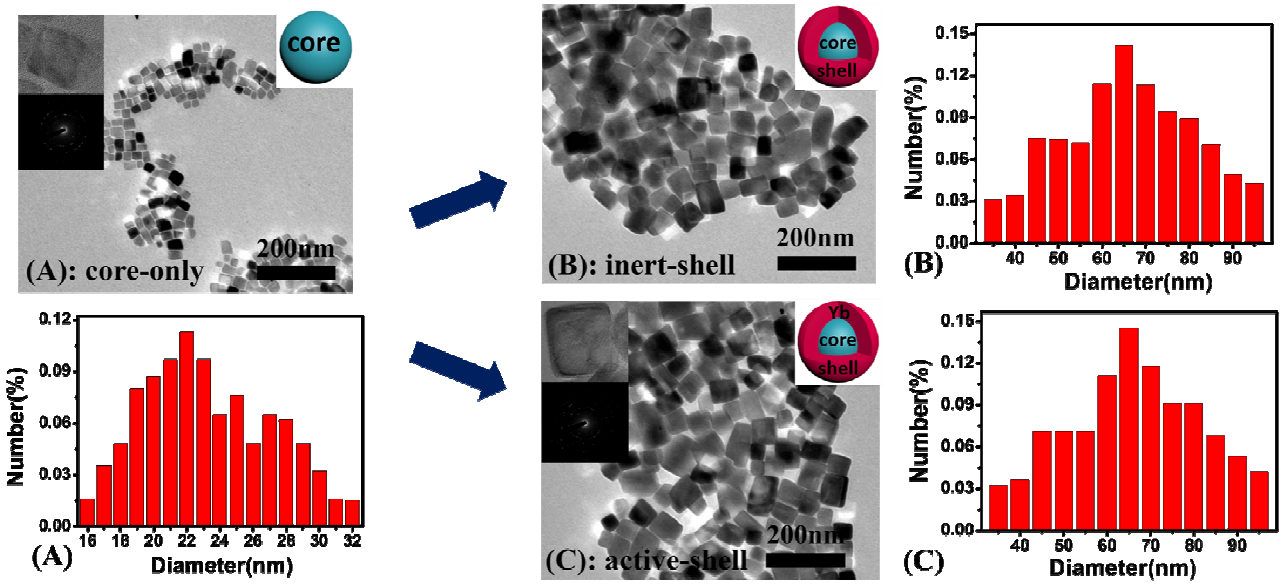

Fig. 2 TEM images and size distribution of (A) $KMnF_3$ core-only NPs, (B) $KMnF_3$: 18 mol% Yb^{3+}, 1 mol% Er^{3+} @ $KMnF_3$ active-core-inert-shell NPs, (C) $KMnF_3$: 18 mol% Yb^{3+}, 1 mol% Er^{3+} @ $KMnF_3$: 2 mol%Yb^{3+} active-core-active-shell NPs. (Insets: corresponding Schematic illustration of (A) $KMnF_3$ core-only NPs, (B) active-core-inert-shell NPs, (C) active-core-active-shell NPs).

We successfully synthesized $KMnF_3$:Yb^{3+}, Er^{3+} (core-only) NPs via a typical solvothermal method, and further prepared $KMnF_3$: 18 mol% Yb^{3+}, 1 mol% Er^{3+} @$KMnF_3$ (active-core-inert-shell) NPs and $KMnF_3$: 18 mol% Yb^{3+}, 1 mol% Er^{3+} @$KMnF_3$: 2 mol% Yb^{3+} (active-core-active-shell) NPs via a coating method. The X-ray powder diffraction (XRD) patterns of the as-synthesized of the samples were showed in **Fig. 1**. The diffraction peaks of the samples can be indexed to cubic phase $KMnF_3$. The diffraction peaks coincide well with the literature values (JCPDS file no. 82-1334).[28] The diffraction peaks at 21.2°, 31.2°, 37.2°, 43.2 °, 48.6°, 53.6° and 67° can be corresponding to (100), (110), (111), (200), (210), (211), and (220) planes (**Fig. 1**). To further confirm the composition of the samples, the energy dispersive X-ray spectrometry (EDX) of the $KMnF_3$: 18 mol% Yb^{3+}, 1 mol% Er^{3+} @$KMnF_3$: 2 mol% Yb^{3+} NPs was measured and shown in **Fig. S3**. The existence of K, Mn, Yb and F elements was clarified by the EDX spectrum (**Fig. S3**). The transmission electron microscopy (TEM) images, high-resolution TEM images, and selected area electron diffraction (SAED) of these samples were showed in **Fig. 2**. The core-only NPs were roughly cube and had uniform morphology. The average size of the core-only NPs, the active-core-inert-shell NPs, and the active-core-active-shell NPs is about 23 ± 5 nm, 65 ± 20 nm, and 65 ± 20 nm respectively, as shown in **Fig. 2**. Note that, the average size of active-core-inert-shell NPs and active-core-active-shell NPs increase obviously after the growth of a shell layer and both the two kinds of core-shell NPs have the similar shell thickness of ~ 40 nm.

3. Results and discussions

3.1 Dependence of the UC properties of $KMnF_3$: 18% Yb^{3+}, x% Er^{3+} NPs on the Er^{3+} concentration

It is known that Yb^{3+} is commonly chosen as a sensitizer for UC

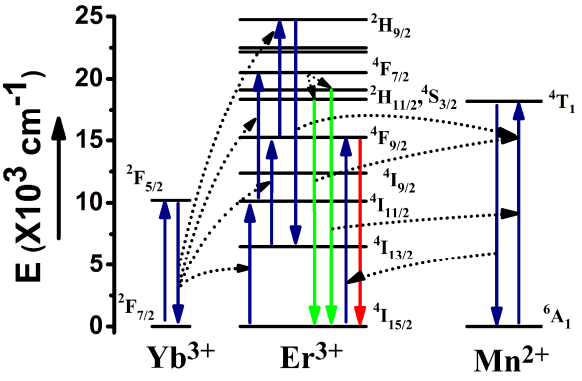

Fig. 3 Energy-level diagram of $KMnF_3$: Yb^{3+}, Er^{3+} NPs, possible up-conversion processes under excitation of a 976 nm laser diode.

materials owing to its large absorption cross-section at 976 nm. In $KMnF_3$: Yb^{3+}, Er^{3+} systems (shown in **Fig. 3**), with the excitation of a 976 nm laser diode, energy transfer from Yb^{3+} to Er^{3+} occurs because of the large spectral overlap between the $^2F_{5/2} \rightarrow {}^2F_{7/2}$ transition of Yb^{3+} and the $^4I_{15/2} \rightarrow {}^4I_{11/2}$ absorption of Er^{3+}, which results in the population of the $^4I_{11/2}$ level. Furthermore, Yb^{3+} ions continuously absorb 976 nm photons and transfer the energy to

Er^{3+} to populate applied high energy levels of Er^{3+} ions: $^4H_{11/2}$ level, $^4F_{9/2}$, $^4F_{7/2}$, and $^2H_{9/2}$. The transitions from the high energy levels to the ground state of Er^{3+} give various UC emissions. Interestingly, by introducing Mn^{2+} into Yb^{3+} and Er^{3+} codoped systems, the $^2H_{11/2} \rightarrow {}^4I_{15/2}$, $^4S_{3/2} \rightarrow {}^4I_{15/2}$, and $^2H_{9/2} \rightarrow {}^4I_{15/2}$ transitions of Er^{3+} are quenched by the following energy transfer between Er^{3+} and Mn^{2+}: $^2H_{11/2}$ ($^4S_{3/2}$) + $^6A_1 \rightarrow {}^4I_{15/2} + {}^4T_1$, $^2H_{9/2} + {}^6A_1 \rightarrow {}^4I_{13/2} + {}^4T_1$ and $^4I_{15/2} + {}^4T_1 \rightarrow {}^4F_{9/2} + {}^6A_1$.[28,32,33] As a result, red UC emission originated from the $^4F_{9/2} \rightarrow {}^4I_{15/2}$ transition of Er^{3+} becomes stronger than that without Mn^{2+}. It is clearly that UC properties of Yb^{3+} Er^{3+} co-doped materials can be affected by the doping concentration of Yb^{3+} and Er^{3+} ions. In our experiments, we first optimized the doping concentration of Yb^{3+} ions in $KMnF_3$ core NPs for obtaining strong red UC emission. The optimized value of molar ratio for Yb^{3+} is about 18% (as shown in **Fig. S4**).

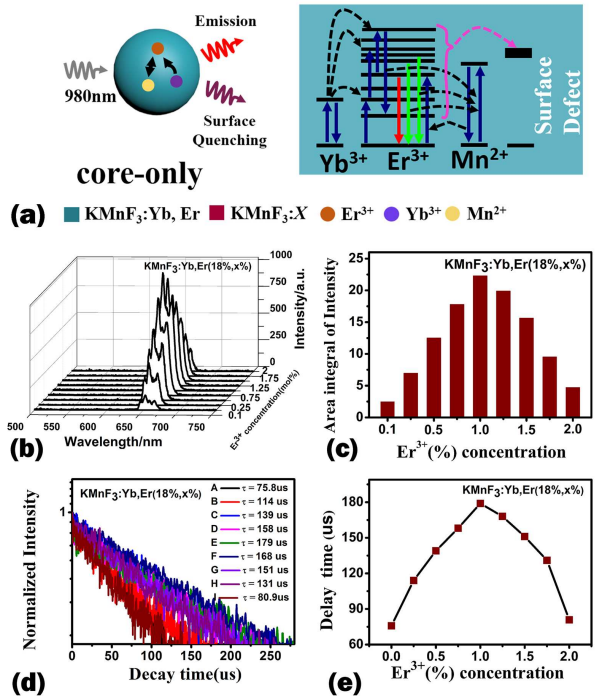

Fig. 4 (a) Schematic illustration and energy transfer mechanisms of the $KMnF_3$ core-only NPs. (b) UC emission spectra of $KMnF_3$: 18% Yb^{3+}, x% Er^{3+} NPs. (c) Intensity enhancement of UC emission depending on the Er^{3+} concentrations in the $KMnF_3$: 18% Yb^{3+}, x% Er^{3+} (x= 0.1, 0.25, 0.5, 0.75, 1, 1.25, 1.5, 1.75, 2) NPs. (d) Photoluminescence decay curves of the $^4F_{9/2}$ level of Er^{3+} in (A-I) $KMnF_3$: 18% Yb^{3+}, x% Er^{3+} (x= 0.1, 0.25, 0.5, 0.75, 1, 1.25, 1.5, 1.75, 2) NPs. (e) Decay time enhancement depending on the Er^{3+} concentrations in the $KMnF_3$: 18% Yb^{3+}, x% Er^{3+} (x= 0.1, 0.25, 0.5, 0.75, 1, 1.25, 1.5, 1.75, 2) NPs.

To investigate the effects of the Er^{3+} concentration on optical properties of NPs, we measured UC emission spectra of $KMnF_3$: 18% Yb^{3+}, x% Er^{3+} NPs with varied Er^{3+} content under the excitation of a 976 nm laser diode with a fixed power density of 65 W cm^{-2}, as shown in **Fig. 4**. The single band emission peaked at 655 nm was observed (shown in **Fig. 4b**), which were attributed to the $^4F_{9/2} \rightarrow {}^4I_{15/2}$ transition of Er^{3+} ions. As aforementioned, the $^2H_{11/2}$, $^4S_{3/2} \rightarrow {}^4I_{15/2}$, $^2H_{9/2} \rightarrow {}^4I_{15/2}$ transitions of Er^{3+} ions were completely quenched by the following energy transfer between Er^{3+} and Mn^{2+}: $^2H_{11/2}$, $^4S_{3/2} + {}^6A_1 \rightarrow {}^4I_{15/2} + {}^4T_1$, $^2H_{9/2} + {}^6A_1 \rightarrow {}^4I_{13/2} + {}^4T_1$ and $^4I_{15/2} + {}^4T_1 \rightarrow {}^4F_{9/2} + {}^6A_1$. As a result, single-band red UC emission originated from the $^4F_{9/2} \rightarrow {}^4I_{15/2}$ transition of Er^{3+} was observed in the above NPs. The dependence of the red emission intensity on the Er^{3+} concentration was shown in **Fig. 4c**. The intensity of the red UC emission increased gradually to the maximum value with increasing the Er^{3+} concentration from 0.1 mol% to 1 mol% since more and more Er^{3+} ions contributed to the red UC emission. Furthermore, the intensity of the red UC emission decreased gradually with increasing the Er^{3+} concentration from 1 mol% to 2 mol% because of the concentration quenching effect of Er^{3+} ions. Thus, the optimum concentration of Er^{3+} was about 1 mol% for the above NPs.

We also measured the lifetime of the $^4F_{9/2}$ level of Er^{3+} in $KMnF_3$: 18% Yb^{3+}, x% Er^{3+} (x = 0.1, 0.25, 0.5, 0.75, 1, 1.25, 1.5, 1.75, 2) NPs by using a 953.6 nm pulsed laser with a pulse width of 10 ns and a repetition rate of 10 Hz as the excitation source. The measured data were shown in **Fig. 4d**. Each of the decay curves can be fitted well with a single-exponential function as $I = I_0 \exp(-t/\tau)$, where I_0 is the initial emission intensity at t = 0 and τ is the lifetime of the monitored level. The lifetime of the $^4F_{9/2}$ level was extended from 75.8 μs to 179 μs with increasing the Er^{3+} concentration from 0.1 % to 1 % and increased to the maximum value when the Er^{3+} concentration was 1 mol% (**Fig. 4e**) owing to the existence of the back energy transfer from Mn^{2+} to Er^{3+}: $^4I_{15/2} + {}^4T_1 \rightarrow {}^4F_{9/2} + {}^6A_1$.[28,32,33] However, the lifetime of the $^4F_{9/2}$ level decreased from 179 μs to 80.9 μs with increasing the Er^{3+} concentration from 1 % to 2 % (**Fig. 4e**) due to the concentration quenching effect. The above results coincided well with the dependence of the red emission intensity on the Er^{3+} concentration (shown in **Fig. 4b**).

3.2 Dependence of the UC properties of $KMnF_3$: 18% Yb^{3+}, 1% Er^{3+} NPs@ $KMnF_3$: x% Yb^{3+} on the Yb^{3+} concentration of the shell

By using $KMnF_3$: 18 mol% Yb^{3+}, 1 mol% Er^{3+} NPs as the core,

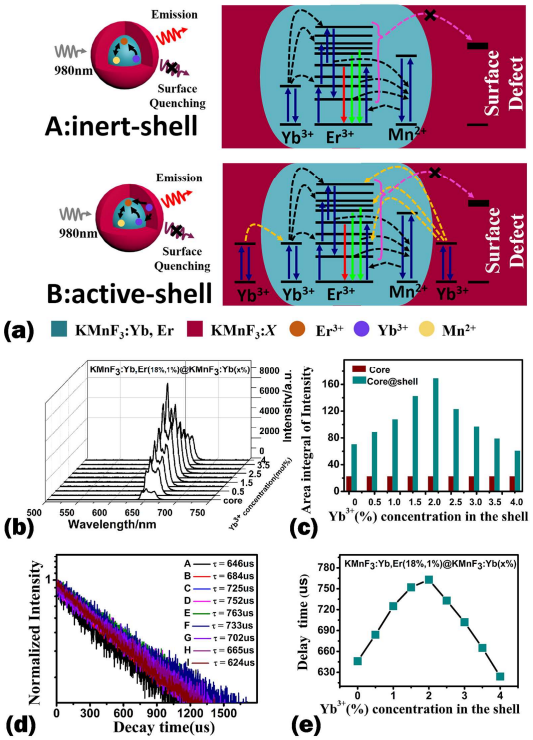

Fig. 5 (a) Schematic illustration and energy transfer mechanisms of (A) active-core-inert-shell NPs, (B) active-core-active-shell NPs. (b) UC emission spectra of $KMnF_3$: 18% Yb^{3+}, 1% Er^{3+}@ $KMnF_3$: x% Yb^{3+} NPs. (c) Intensity enhancement of UC emission depending on the Yb^{3+} concentrations in the $KMnF_3$: 18% Yb^{3+}, 1% Er^{3+}@ $KMnF_3$: x% Yb^{3+} (x= 0, 0.5, 1, 1.5, 2, 2.5, 3, 3.5, 4) NPs. (d) Photoluminescence decay curves of the $^4F_{9/2}$ level of Er^{3+} in (A-I) $KMnF_3$: 18% Yb^{3+}, 1% Er^{3+}@ $KMnF_3$: x% Yb^{3+} (x= 0, 0.5, 1, 1.5, 2, 2.5, 3, 3.5, 4) NPs. (e) Decay time enhancement depending on the Er^{3+} concentrations in the $KMnF_3$: 18% Yb^{3+}, 1% Er^{3+}@ $KMnF_3$: x% Yb^{3+} (x= 0, 0.5, 1, 1.5, 2, 2.5, 3, 3.5, 4) NPs.

Cite this: DOI: 10.1039/coxx00000x

www.rsc.org/xxxxxx

ARTICLE TYPE

we prepared $KMnF_3$: 18 mol% Yb^{3+}, 1 mol% Er^{3+}@$KMnF_3$: Yb^{3+} active-core-active-shell NPs with varied Yb^{3+} concentration in the shell. To clarify the effects of the Yb^{3+} concentration in the shell on optical properties of NPs, we measured UC emission spectra of $KMnF_3$: 18 mol% Yb^{3+}, 1 mol% Er^{3+}@$KMnF_3$: Yb^{3+} NPs with varied Yb^{3+} concentration in the shell under the excitation of a 976 nm laser diode, as shown in **Fig. 5**. After coating an inert shell $KMnF_3$ on the core NPs, the red UC emission were enhanced by 3.1 times compared to that of the core-only NPs owing to the well-known surface passivation effect of the shell.[34] In the case of $KMnF_3$: 18 mol% Yb^{3+}, 1 mol% Er^{3+}@$KMnF_3$: Yb^{3+} active-core-active-shell NPs, the intensity of the red UC emissions increased monotonically to the corresponding maximum value with increasing the Yb^{3+} concentration of the shell from zero to 2 mol%. Furthermore, the intensity of the UC emissions decreased gradually with increasing the Yb^{3+} concentration of the shell from 2 % to 4 %. Thus, the optimum concentration of Yb^{3+} in the shell was about 2 mol% for the active-core-active-shell NPs. The above results showed that by doping a certain amount (e.g., ~ 2 mol%) of Yb^{3+} ions into the shell, the red UC emissions of the active-core-active-shell NPs was further improved by 2.4 times compared to that of the active-core-inert-shell NPs since the Yb^{3+} ions in the shell could transfer energy from the pump source to the core and make a contribution to the red UC emissions.[8,35] However, if the Yb^{3+} concentration in the shell was too high (> 2 mol%), the Yb^{3+} ions in the shell would preclude the core region from 976 nm excitation and also the concentration quenching effect occurred, causing the weakening of the red UC emissions. In addition, we also measured the lifetime of the $^4F_{9/2}$ level of Er^{3+} in $KMnF_3$: 18 mol% Yb^{3+}, 1 mol% Er^{3+}@$KMnF_3$: Yb^{3+} NPs with varied Yb^{3+} concentration in the shell by using a 953.6 nm pulsed laser with a pulse width of 10 ns and a repetition rate of 10 Hz as the excitation source. The lifetimes were shown in **Fig. 5d**. By growing an inert shell on the core NP, the lifetime of the $^4F_{9/2}$ level was extended from 179 μs to 646 μs, owing to the reduction of the nonradiative relaxation rate caused by the surface passivation effect. Interestingly, for the active-core-active-shell NPs, the lifetime of the $^4F_{9/2}$ level increased monotonically to the corresponding maximum value with increasing the Yb^{3+} concentration of the shell from zero to 2 mol%. In addition, the lifetime decreased gradually with increasing the Yb^{3+} concentration of the shell from 2 % to 4 % (**Fig. 5d** and **Fig. 5e**). The above results showed that by doping a certain amount (e.g., ~ 2 mol%) of Yb^{3+} ions into the shell, the lifetime of the $^4F_{9/2}$ level of Er^{3+} ions in the active-core-active-shell NPs was further increased to 763 μs by introducing Yb^{3+} ions into the shell to form the active shell. In this case, there are two factors that contribute to the increase of the lifetime. One is the surface passivation effect. The other is originated from Yb^{3+} ions inside the shell. Since the Yb^{3+} concentration of the shell was lower than that of the core region, the lifetime of the $^2F_{5/2}$ level of Yb^{3+} in the shell would be longer than that in the core region.[36,37] Generally, the measured lifetime of the $^4F_{9/2}$ level of Er^{3+} in Yb^{3+} and Er^{3+} codoped systems pumped at 953.6 nm is related to the lifetime of the $^2F_{5/2}$ level of Yb^{3+} owing to the existence of energy transfer from Mn^{2+} to Er^{3+}. The above results showed that strong red UC emission could be achieved in the active-core-active-shell NPs by growing the active shell layer on the core-only NPs.

3.3 Optical amplification at 650 nm in a polymer-based waveguide amplifier based on $KMnF_3$: Yb^{3+}, Er^{3+} @ $KMnF_3$: Yb^{3+} active-core-active-shell NPs

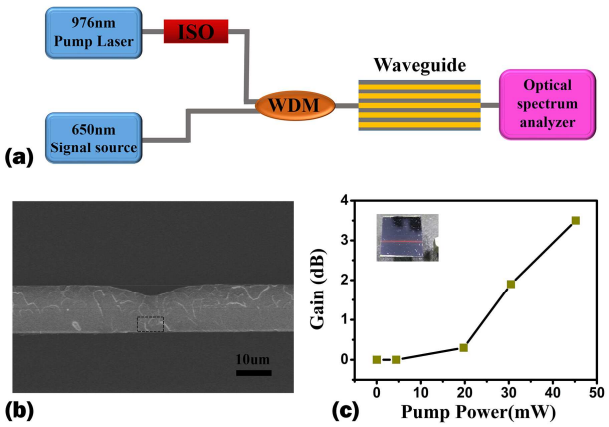

Fig. 6 (a) Experimental setup for measuring the optical gain of waveguide amplifiers. SEM micrograph of the waveguide. (b) The cross section of the waveguide after embedding the active-core-active-shell NPs-PMMA into the groove. (c) Gain as a function of pump power (976 nm) in in a 17 mm-long the active-core-active-shell NPs-doped waveguide (Insets: corresponding luminescent photos of waveguide amplifiers).

By dispersing the active-core-active-shell NPs into PMMA as the gain medium (**Fig. S5**) and embedding this gain medium into a polymer groove, we constructed a polymer-based waveguide amplifier based on the UCNPs (**Fig. S6**).[38-40] **Fig. 6a** shows the schematic of the experimental setup for the optical gain measurement of the waveguide amplifier. A 650 nm laser diode was used as the signal source and a 976 nm laser diode was used as the pump source. The signal and pump light were launched into the channel waveguides by a 980/650 nm wavelength division multiplexing (WDM) coupler. The output light from the device was collected and coupled to an optical spectrum analyzer (OSA, ANDO AQ-6315A). **Fig. 6b** shows the SEM micrograph of the cross-section of the waveguide after embedding the active-core-active-shell NPs dispersed PMMA into the groove. The relative gain was calculated using the formula,

$$Gain[dB] = 10log\left(\frac{P^{p}_{s-out}}{P_{s-out}}\right) = 10\log(P^{p}_{s-out}) - 10\log(P_{s-out}) \quad ,$$

where P^{p}_{s-out} was the output signal powers in cases with pump light and P_{s-out} was the output signal powers in cases without pump light.[46] **Fig. 6c** shows the relative gain as a function of pump power for the signal wavelengths. For an input signal power of 0.3 mW, the relative gain of the waveguide amplifier increased with increasing the pump power. When the pump power was 45.2 mW, the maximum relative optical gain at 650 nm was ~ 3.5 dB. This is the first report on optical amplification at 650 nm in the polymer-based waveguide amplifier based on UC NPs, to the best of our knowledge.

4. Conclusion

In summary, we constructed polymer-based waveguide amplifiers using $KMnF_3$: Yb^{3+}, Er^{3+} @ $KMnF_3$: Yb^{3+} active-core-active-shell UCNPs doped polymer as gain media and got a relative optical gain of ~ 3.5 dB at 650 nm in the polymer waveguides pumped by a 976 nm laser diode for the first time. Compared with the traditional polymer waveguide amplifiers operating at 650 nm pumped by UV light, such UC NPs doped polymer waveguide amplifiers can be pumped by NIR light, which efficiently decreases the photo damage to the polymer matrix of devices. Therefore, this kind of UC NPs doped polymer waveguide amplifiers has potential applications in short distance telecommunication systems, such as automobile optical LANs. The UC $KMnF_3$: 18 mol% Yb^{3+}, 1 mol% Er^{3+}@$KMnF_3$: 2 mol%Yb^{3+} NPs (active-core-active-shell) were synthesized by coating an active-layer shell containing Yb^{3+} ions. In comparison with optical properties of the $KMnF_3$: 18 mol% Yb^{3+}, 1 mol% Er^{3+} core-only NPs, the intensities of red UC fluorescence were enhanced by 7.5 times after coating active shell ($KMnF_3$: Yb^{3+}) on the $KMnF_3$: 18 mol% Yb^{3+}, 1 mol% Er^{3+} NPs. By using the $KMnF_3$: 18 mol% Yb^{3+}, 1 mol% Er^{3+} @ $KMnF_3$: 2 mol% Yb^{3+} NPs as the gain medium, we constructed polymer waveguide amplifiers based on UCNPs. A relative optical gain of ~ 3.5 dB was obtained at 650 nm in the 17 mm-long waveguide when the power of the 976 nm LD was increased to ~45.2 mW. In the future, we will explore novel ways to increase the upconversion efficiency of UCNPs or the doping concentration of UCNPs in the polymer waveguide for further improving the performance of the polymer waveguide amplifiers based on UCNPs.

Acknowledgments

This work was supported by NSFC (grants 61178073, 11274139, 61222508, 61275189, 61378004, 61527823, 60908001, 61077033, 51072065, 60908031, 61475061, and 61261130586).

Notes and references

State Key Lab on Integrated Optoelectronics, College of Electronic Science & Engineering, Jilin University, Changchun 130012, China. Fax: +86 4318516 8241; Tel: +86 431 8516 8325; E-mail: dzhao@jlu.edu.cn; qings@jlu.edu.cn; wpqin@jlu.edu.cn .

† Electronic Supplementary Information (ESI) available

1. Guo-Bin Shan, George P. Demopoulos, Adv. Mater., 2010, 22, 4373
2. Weiping Qin, Daisheng Zhang, Dan Zhao, Lili Wang, Kezhi Zheng, Chem. Commun., 2010, 46, 2304
3. Feng Wang, Yu Han, Chin Seong Lim, Yunhao Lu, Juan Wang, Jun Xu, Hongyu Chen, Chun Zhang, Minghui Hong, Xiaogang Liu, Nature, 2010, 463, 1061.
4. Wei Zheng, Shanyong Zhou, Zhuo Chen, Ping Hu, Yongsheng Liu, Datao Tu, Haomiao Zhu, Renfu Li, Mingdong Huang, Xueyuan Chen, Angew. Chem. Int. Ed., 2013, 125, 6803.
5. Jianan Liu, Jiwen Bu, Wenbo Bu, Shengjian Zhang, Limin Pan, Wenpei Fan, Feng Chen, Liangpin Zhou, Weijun Peng, Kuaile Zhao, Jiulin Du, Jianlin Shi, Angew. Chem. Int. Ed., 2014, 53, 4551
6. Liang Cheng, Kai Yang, Shuai Zhang, Mingwang Shao, Shuittong Lee, Zhuang Liu, Nano Res., 2010, 3(10), 722
7. Guanying Chen, Tymish Y. Ohulchanskyy, Wing Cheung Law, Hans Agrenb, Paras N. Prasad, Nanoscale, 2011, 3, 2003.
8. Fiorenzo Vetrone, Rafik Naccache, Venkataramanan Mahalingam, Christopher G. Morgan, John A. Capobianco, Adv. Funct. Mater., 2009,19, 2924
9. Guanying Chen, Jie Shen, Tymish Y. Ohulchanskyy, Nayan J. Patel, Artem Kutikov, Zhipeng Li, Jie Song, Ravindra K. Pandey, Hans Agren, Paras N. Prasad, Gang Han, ACS Nano, 2012, 6(9), 8280
10. Yu Wang, Langping Tu, Junwei Zhao, Yajuan Sun, Xianggui Kong, Hong Zhang, J. Phys. Chem. C, 2009, 113, 7164.
11. Hon-Tung Wong, Fiorenzo Vetrone, Rafik Naccache, Helen Lai Wa Chan, Jianhua Hao, John A. Capobianco, J. Mater. Chem., 2011, 21, 16589
12. Guanying Chen, Tymish Y. Ohulchanskyy, Sha Liu, Wing-Cheung Law, FangWu, Mark T. Swihart, Hans Agren, Paras N. Prasad, ACS Nano, 2012, 6(4), 2969.
13. Shan Jin, Liangjun Zhou, Zhanjun Gu, Gan Tian, Liang Yan, Wenlu Ren, Wenyan Yin, Xiaodong Liu, Xiao Zhang, Zhongbo Hu,Yuliang Zhao, Nanoscale, 2013, 5(23), 11910.
14. Wenlu Ren, Gan Tian, Shan Jian, Zhanjun Gu, Liangjun Zhou, Liang Yan, Shan Jin, Wenyan Yin, Yuliang Zhao, RSC Advances, 2012, 2, 7037.
15. Shili Gai, Piaoping Yang, Xingbo Li, Chunxia Li, Dong Wang, Yunlu Dai, Jun Lin, J. Mater. Chem., 2011, 21, 14610.
16. Wenjuan Zhu, Daqin Chen, Lei Lei, Ju Xua, Yuansheng Wang, Nanoscale,2014, 6, 10500.
17. S.H. Bo, J. Hu, Z. Chen, Q. Wang, G.M. Xu, X.H. Liu, Z. Zhen, Appl. Phys. B, 2009, 97, 665.
18. Bo S. Wang, J. Zhao, H. Zhao, H. Ren, Q. Wang, G.Xu, X. Zhang, X. Liu, Z. Zhen, Appl. Phys. B, 2008, 91(1), 79.
19. Wai-Sum Lo, Wai-Ming Kwok, Ga-Lai Law, Chi-Tung Yeung, Chris Tsz-Leung Chan, Ho-Lun Yeung, Hoi-Kuan Kong, Chi-Hang Chen, Margaret B. Murphy, Ka-Leung Wong, Wing-Tak Wong, Inorg. Chem., 2011, 50, 5309.
20. Ga-Lai Law, Wai-Ming Kwok, Wing-Tak Wong, J. Phys. Chem. B, 2007, 111(37), 10858.
21. Xun Wang, Jing Zhuang, Qing Peng, Yadong Li, Nature, 2005, 437, 121.
22. Manabu Kagami, Optical Technologies For Car Applications Innovation of the optical waveguide device fabrication. Optical communications-perspectives on next generation technologies. October 23-25, 2007.
23. Guanshi Qin, Tatsuya Yamashita, Yusuke Arai, Takenobu Suzuki, Yasutake Ohishi, Opt. Commun., 2007, 279(2), 298.
24. J. Goudeau, G. Widawski, M. Rossback, B. Bareel, P. Helvenstein, and L. Huff, Proceedings of the International Plastic Optical Fiber Conference. International Cooperative of Plastic Optical Fibres, 2004.
25. Hao Liang, Qijin Zhang, Zhiqiang Zheng, Hai Ming, Zengchang Li, Jie Xu, Biao Chen, Hui Zhao, Opt. Lett., Vol. 29, 2004, 5, 477.
26. Zhiqiang Zheng, Hai Ming, Xiaohong Sun, Jun Yang, Donguo Zhang, Jianping Xie, Hao Liang, Qijin Zhang, Zebo Zhang, Li Cao, Anlian Pan, J. Opt. Soc. Am. B, 2005, 22(4), 820.
27. Kwok Chu Tsang, Chun-Yuen Wong, Edwin Yue Bun Pun, Opt. Lett., 2010, 35(4), 520.
28. Juan Wang, Feng Wang, Chao Wang, Zhuang Liu, Xiaogang Liu, Angew. Chem. Int. Edit., 2011, 50(44), 10369.
29. Xun Wang, Jing Zhuang, Qing Peng, Yadong Li, Nature, 2005, 437(7055), 121.
30. Dan Zhao, Huan Chen, Kezhi Zheng, Xiaohong Chuai, Fangda Yu, Hui Li, Changfeng Wu, Guanshi Qin, Weihua Di, Weiping Qin, RSC Adv., 2014, 4, 13490.
31. Markus Haase, Helmut Schafer, Angew. Chem. Int. Edit., 2011, 50(26), 5808.
32. D. D. Sell, R. L. Greene, Robert M. White, Phys. Rev., 1967, 158, 489.
33. J.M. Flaherty, B. Di Bartolo, J. Lumin., 1973, 8(1), 51.
34. John-Christopher Boyer, Jacinthe Gagnon, Louis A. Cuccia, John A. Capobianco, Chem. Mater., 2007, 19(14), 3358.
35. Daqin Chen, Yunlong Yu, Feng Huang, Hang Lin, Ping Huang, Anping Yang, Zhaoxing Wang, Yuansheng Wang, J. Mater. Chem., 2012, 22, 2632.

Cite this: DOI: 10.1039/coxx00000x

www.rsc.org/xxxxxx

ARTICLE TYPE

36. Peizhi Yang, Peizhen Deng, Zhiwen Yin, J. Lumin., 2002, 97, 51
37. D. S. Sumida, Opt. Lett., 1994, 17, 1343
38. Cong Chen, Dan Zhang, Tong Li, Daming Zhang, Limei Song, Zhen Zhen, Appl. Phys. Lett.,2009, 94, 041119.
39. Tianjiao Wang, Dan Zhao, Meiling Zhang, Jiao Yin, Weiye Song, Zhixu Jia, Xibin Wang, Guanshi Qin, Weiping Qin, Fei Wang, Daming Zhang, Opt. Mater. Express, 2015, 5(3), 469.
40. Dan Zhang, Cong Chen, Changming Chen, Chunsheng Ma, Daming Zhang, Appl. Phys. Lett., 2007, 91, 161109.